

# **Supplementary Material: Specular Highlight Removal in Facial Images**

Chen Li<sup>1\*</sup>    Stephen Lin<sup>2</sup>    Kun Zhou<sup>1</sup>    Katsushi Ikeuchi<sup>2</sup>  
<sup>1</sup>State Key Lab of CAD&CG, Zhejiang University    <sup>2</sup>Microsoft Research

## **1. Computation of skin relative absorbance vectors $\sigma_m$ and $\sigma_h$**

Skin albedo  $\mathbf{A}$  can be expressed by a combination of two pigments, melanin and hemoglobin, as

$$\mathbf{A}(p) = \sigma_m^{\rho_m(p)} \sigma_h^{\rho_h(p)}, \quad (1)$$

where  $\rho_m(p)$ ,  $\rho_h(p)$ ,  $\sigma_m$ ,  $\sigma_h$  are the pigment densities and relative absorbance vectors of melanin and hemoglobin, respectively.

In solving for the relative absorbance vectors  $\sigma_m$ ,  $\sigma_h$ , we first apply the logarithm operation to Eq. (1):

$$\log \mathbf{A}(p) = \rho_m(p) \log \sigma_m + \rho_h(p) \log \sigma_h. \quad (2)$$

Different  $\log \mathbf{A}$  with different pigment densities thus lie in a plane  $\mathbb{P}$  in the log-RGB space with two bias vectors  $\log \sigma_m$  and  $\log \sigma_h$  as shown in Fig. 1(a).

To compute the two bias vectors, which are assumed to be invariant from person to person, we use the face dataset in [12]. Diffuse skin patches under a neutral illumination color are first extracted using the method in [1]. We then use the intrinsic image decomposition of [12] to extract the skin albedo without diffuse shading. According to Eq. (2), all the decomposed skin albedo values ideally lie in a plane  $\mathbb{P}$  formed by  $\log \sigma_m$  and  $\log \sigma_h$  in log-RGB space. However, since slight shading variations likely still exist in the decomposed albedo skin samples, the skin albedo values will not lie in a perfect plane. So we use Principal Components Analysis to extract the plane  $\mathbb{P}$  and project all skin samples onto  $\mathbb{P}$  along the shading direction  $\mathbf{1} = (1, 1, 1)^T$  in log-RGB space to remove the shading effects. After this projection onto  $\mathbb{P}$ , Independent Components Analysis is applied on the projected skin albedo samples to extract the two independent bias vectors. We compute the bias vectors for each skin patch and use the average as the value of  $\log \sigma_m$  and  $\log \sigma_h$ . Figure 1(b) shows varying skin albedos with different melanin and hemoglobin densities using the computed melanin absorbance vector  $\sigma_m$  and hemoglobin absorbance vector  $\sigma_h$ .

\*This work was done while Chen Li was an intern at Microsoft Research.

Among all the examined skin patches, the (average, standard derivation) of angular differences between their estimated bias vectors and the average values of  $\log \sigma_m$  and  $\log \sigma_h$  are  $(3.70^\circ, 2.33^\circ)$  and  $(9.61^\circ, 8.68^\circ)$ , respectively. Based on this empirical study and claims in [10],  $\sigma_m$  and  $\sigma_h$  can be treated as approximately the same among different people, and variations in skin color are mainly caused by differences in pigment densities  $\rho$ .

## **2. Uniform Illumination Chromaticity Estimation**

Although our method is formulated to estimate directionally variant illumination, we can compare it with techniques for estimating a uniform illumination chromaticity. We specifically compare to IIC [9], SpePL [2], FacePL [6] and FaceGM [1]. IIC [9] assumes a direct correlation between illumination chromaticity and image chromaticity in inverse-intensity chromaticity space. SpePL [2] combines the dichromatic model with a hard Planckian locus constraint. FacePL [6] utilizes a soft Planckian locus constraint and a statistical skin albedo distribution. FaceGM [1] uses gamut mapping with a generic statistical model of skin color to estimate the illumination color. All of the comparison methods are able to handle only uniform illumination chromaticity.

For a quantitative comparison, we use the reprocessed version of Gehler’s ColorChecker dataset [3] provided by [7], where the images have linear camera responses and calibrated illumination color. From this dataset, we manually select all of the 37 facial images that contain specular reflection and use them for evaluation. We use the error metric suggested by Hordley and Finlayson [4]:

$$e = \arccos\left(\frac{\Gamma_e^T \Gamma_m}{\|\Gamma_e\| \|\Gamma_m\|}\right), \quad (3)$$

which measures the angle between the RGB triplets of estimated illumination  $\Gamma_e$  and ground truth illumination  $\Gamma_m$ .

The measured angular errors of the proposed method as well as the comparison methods are listed in Tab. 1, including the minimum, median, mean, maximum and standard

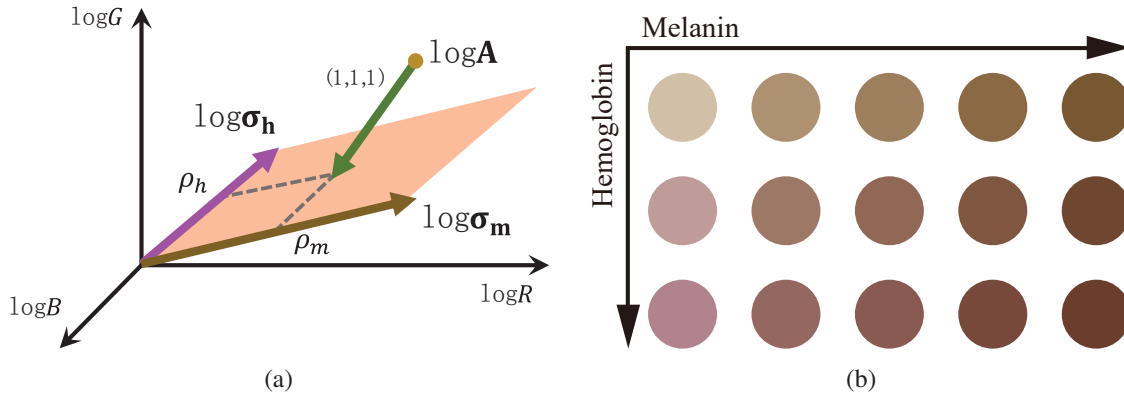


Figure 1. Melanin-hemoglobin based skin model in log-RGB space. (a) In the log-RGB space, the log of the melanin absorbance vector  $\sigma_m$  and hemoglobin absorbance vector  $\sigma_h$  forms a plane. (b) Varying skin albedos with different combinations of melanin and hemoglobin density.

Table 1. Angular error measurement for illumination chromaticity estimation

Algorithm	Min	Median	Mean	Max	Std
IIC [9]	1.90	7.12	8.12	15.1	3.63
SpePL [2]	0.17	2.85	2.89	6.25	1.50
FacePL [6]	3.08	4.49	4.98	9.70	1.75
FaceGM [1]	<b>0.02</b>	3.80	3.96	8.21	1.84
Ours	<b>0.02</b>	<b>0.76</b>	<b>0.88</b>	<b>3.43</b>	<b>0.77</b>

derivation of the errors. The overall performance of our approach surpasses the others, with greater robustness as indicated by the standard deviation of errors. A few estimation results are shown in Fig. 2, and the rest are provided in Fig. 3-Fig. 8. The ground truth is given in the last column of these figures.

Because of their Planckian locus constraints, SpePL and FacePL have larger estimation errors when the lighting de-

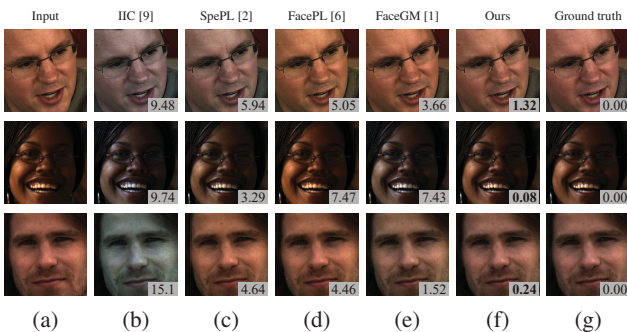


Figure 2. Some results for illumination chromaticity estimation. (a) Input images. (b/c/d/e/f/g) Illumination corrected images with the chromaticity estimated using (b) IIC [9], (c) SpePL [2], (d) FacePL [6], (e) FaceGM [1], (f) our method, and (g) calibrated ground truth using a ColorChecker. Measured errors are listed in the lower right corners.

viates from the Planckian assumption, such as in the first row of Fig. 2. FaceGM is relatively less stable, as reflected by its higher standard deviation in Tab. 1, since its gamut mapping approach may lead to a large range of feasible illumination chromaticities, especially for dark skin colors such as in the second row of Fig. 2, which have a relatively narrow gamut. The performance of IIC is limited by the accuracy of specular-diffuse segmentation, which is often challenging for human skin, especially where highlights may be subtle, such as in the third row of Fig. 2. Although our method also utilizes specular highlights for estimating illumination chromaticity, it is still effective in cases where specular highlights are weak because of the melanin-hemoglobin based skin model.

### 3. Additional Results for Specular Highlight Removal

In Figure 9-Fig. 13, we present additional results for specular highlight removal using all 37 facial images that contain visible specular highlights in Gehler’s ColorChecker dataset [3, 7]. In each figure, column (a) is the input image; columns (b/c/d/e/f) are the separated diffuse images by (b) ILD[8], (c) MDCBF[11], (d) DarkP[5], (e) FacePL[6], and (f) our method.

### References

- [1] S. Bianco and R. Schettini. Adaptive color constancy using faces. *IEEE Trans. Patt. Anal. and Mach. Intel.*, 36(8):1505–1518, 2014.
- [2] G. D. Finlayson and G. Schaefer. Solving for colour constancy using a constrained dichromatic reflection model. *Int. Journal of Computer Vision*, 42:127–144, 2001.

- [3] P. V. Gehler, C. Rother, A. Blake, T. Minka, and T. Sharp. Bayesian color constancy revisited. pages 1–8, 06 2008.
- [4] S. D. Hordley and G. D. Finlayson. Re-evaluating colour constancy algorithms. In *ICCV*, pages 76–79, 2004.
- [5] H. Kim, H. Jin, S. Hadap, and I. Kweon. Specular reflection separation using dark channel prior. In *CVPR*, pages 1460–1467, 2013.
- [6] C. Li, K. Zhou, and S. Lin. Intrinsic face image decomposition with human face priors. In *ECCV (5)'14*, pages 218–233, 2014.
- [7] S. Lynch, M. Drew, and G. Finlayson. Colour constancy from both sides of the shadow edge. In *Computer Vision Workshops (ICCVW), 2013 IEEE International Conference on*, pages 899–906, 2013.
- [8] R. Tan and K. Ikeuchi. Separating reflection components of textured surfaces using a single image. *IEEE Trans. Patt. Anal. and Mach. Intel.*, 27(2):178–193, 2005.
- [9] R. T. Tan, K. Nishino, and K. Ikeuchi. Color constancy through inverse-intensity chromaticity space. *J. Opt. Soc. Am. A*, 21(3):321–334, Mar 2004.
- [10] N. Tsumura, N. Ojima, K. Sato, M. Shiraishi, H. Shimizu, H. Nabeshima, S. Akazaki, K. Hori, and Y. Miyake. Image-based skin color and texture analysis/synthesis by extracting hemoglobin and melanin information in the skin. *ACM Trans. Graph.*, 22(3):770–779, July 2003.
- [11] Q. Yang, S. Wang, and N. Ahuja. Real-time specular highlight removal using bilateral filtering. In *ECCV*, volume 6314, pages 87–100. 2010.
- [12] Q. Zhao, P. Tan, Q. Dai, L. Shen, E. Wu, and S. Lin. A closed-form solution to retinex with nonlocal texture constraints. *IEEE Trans. Patt. Anal. and Mach. Intel.*, 34(7):1437–1444, July 2012.

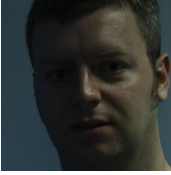
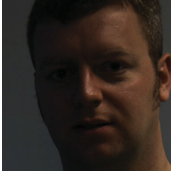
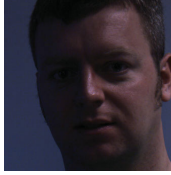
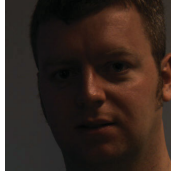
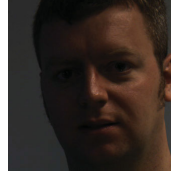
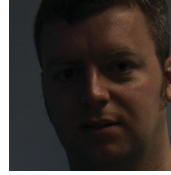
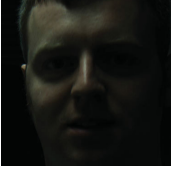
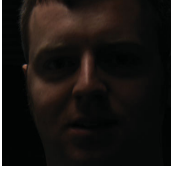
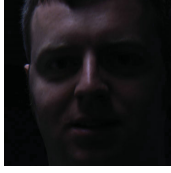
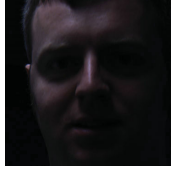
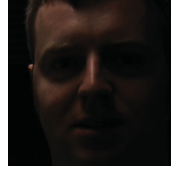
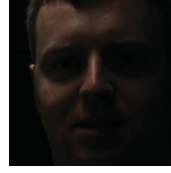
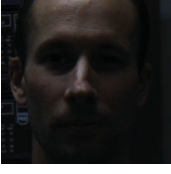
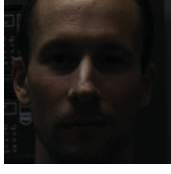
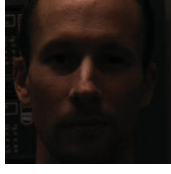
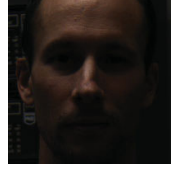
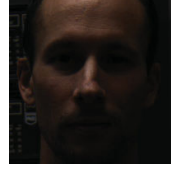
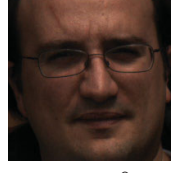
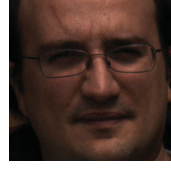
Input	IIC [9]	SpePL [2]	FacePL [6]	FaceGM [1]	Ours	Ground truth
						
	7.12°	1.10°	3.86°	4.74°	<b>1.87°</b>	0.00°
						
	3.31°	2.63°	3.72°	4.05°	<b>0.19°</b>	0.00°
						
	6.93°	1.11°	4.81°	4.93°	<b>2.26°</b>	0.00°
						
	8.27°	2.14°	3.82°	5.31°	<b>0.42°</b>	0.00°
						
	6.27°	2.58°	3.48°	3.76°	<b>0.06°</b>	0.00°
						
	9.74°	3.29°	7.47°	7.43°	<b>0.08°</b>	0.00°
						
	14.2°	2.32°	4.74°	4.17°	<b>0.62°</b>	0.00°
(a)	(b)	(c)	(d)	(e)	(f)	(g)

Figure 3. Additional results for illumination chromaticity estimation. (a) Input images. (b/c/d/e/f/g) Illumination corrected images with the chromaticity estimated by using (b) IIC [9], (c) SpePL [2], (d) FacePL [6], (e) FaceGM [1], (f) our method, and (g) calibrated ground truth using a ColorChecker. Below each corrected image is the measured error of the estimated illumination chromaticity.



Figure 4. Additional results for illumination chromaticity estimation. (a) Input images. (b/c/d/e/f/g) Illumination corrected images with the chromaticity estimated by using (b) IIC [9], (c) SpePL [2], (d) FacePL [6], (e) FaceGM [1], (f) our method, and (g) calibrated ground truth using a ColorChecker. Below each corrected image is the measured error of the estimated illumination chromaticity.

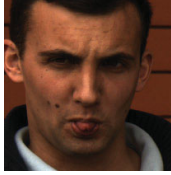
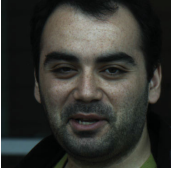
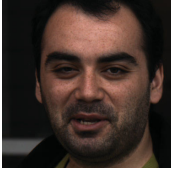
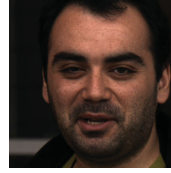
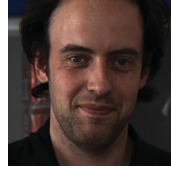
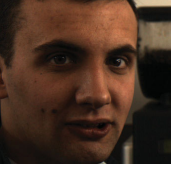
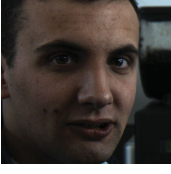
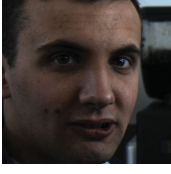
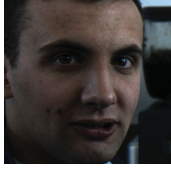
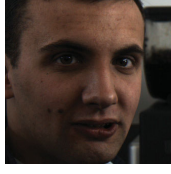
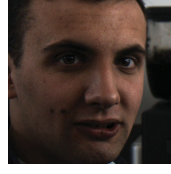
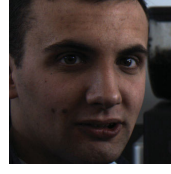
Input	IIC [9]	SpePL [2]	FacePL [6]	FaceGM [1]	Ours	Ground truth
						
	5.26°	3.23°	3.89°	<b>0.02°</b>	0.71°	0.00°
						
	13.4°	2.96°	4.49°	4.30°	<b>1.26°</b>	0.00°
						
	10.8°	2.85°	4.59°	1.51°	<b>0.99°</b>	0.00°
						
	9.63°	2.74°	8.90°	7.96°	<b>0.63°</b>	0.00°
						
	1.90°	1.61°	3.81°	3.70°	<b>3.43°</b>	0.00°
						
	9.94°	3.08°	3.09°	2.55°	<b>0.93°</b>	0.00°
						
	9.50°	5.94°	5.05°	3.66°	<b>1.32°</b>	0.00°
(a)	(b)	(c)	(d)	(e)	(f)	(g)

Figure 5. Additional results for illumination chromaticity estimation. (a) Input images. (b/c/d/e/f/g) Illumination corrected images with the chromaticity estimated by using (b) IIC [9], (c) SpePL [2], (d) FacePL [6], (e) FaceGM [1], (f) our method, and (g) calibrated ground truth using a ColorChecker. Below each corrected image is the measured error of the estimated illumination chromaticity.

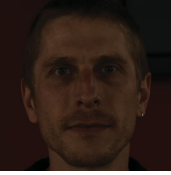
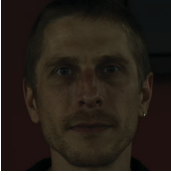
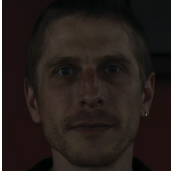
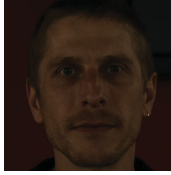
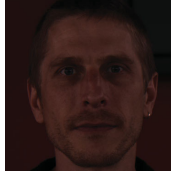
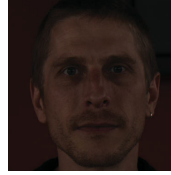
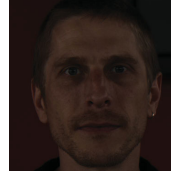
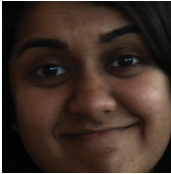
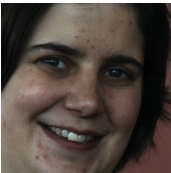
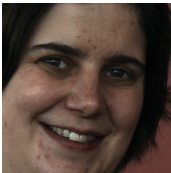
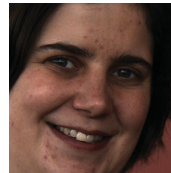
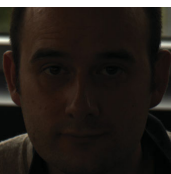
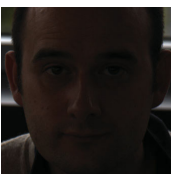
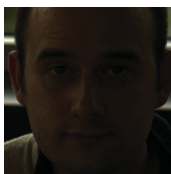
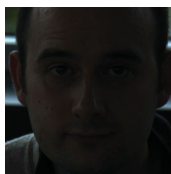
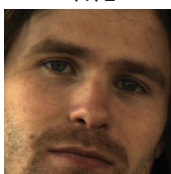
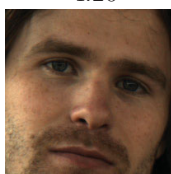
Input	IIC [9]	SpePL [2]	FacePL [6]	FaceGM [1]	Ours	Ground truth
						
	4.67°	5.76°	6.10°	4.99°	<b>0.60°</b>	0.00°
						
	4.72°	2.38°	3.69°	2.60°	<b>1.02°</b>	0.00°
						
	7.57°	4.18°	6.03°	3.81°	<b>0.86°</b>	0.00°
						
	4.04°	2.86°	7.72°	4.20°	<b>0.86°</b>	0.00°
						
	9.38°	3.80°	5.42°	3.52°	<b>0.23°</b>	0.00°
						
	6.13°	2.87°	5.73°	4.58°	<b>1.11°</b>	0.00°
						
	6.86°	2.50°	9.64°	8.21°	<b>0.06°</b>	0.00°
(a)	(b)	(c)	(d)	(e)	(f)	(g)

Figure 6. Additional results for illumination chromaticity estimation. (a) Input images. (b/c/d/e/f/g) Illumination corrected images with the chromaticity estimated by using (b) IIC [9], (c) SpePL [2], (d) FacePL [6], (e) FaceGM [1], (f) our method, and (g) calibrated ground truth using a ColorChecker. Below each corrected image is the measured error of the estimated illumination chromaticity.

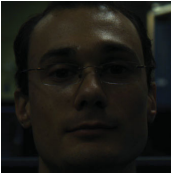
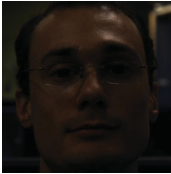
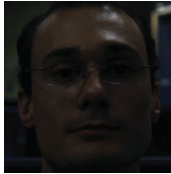
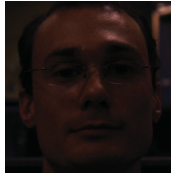
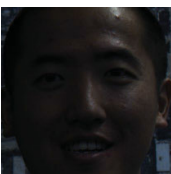
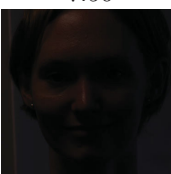
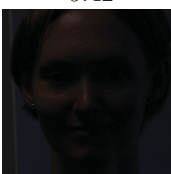
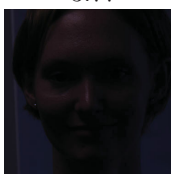
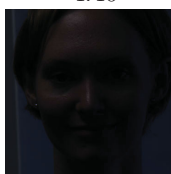
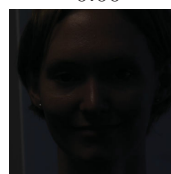
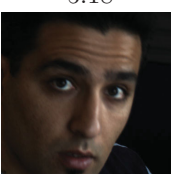
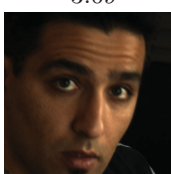
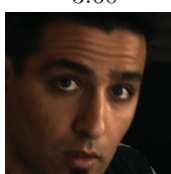
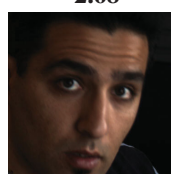
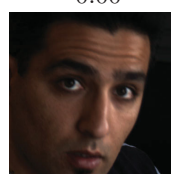
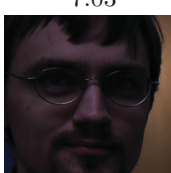
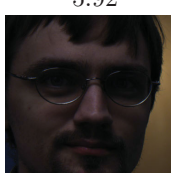
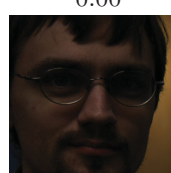
Input	IIC [9]	SpePL [2]	FacePL [6]	FaceGM [1]	Ours	Ground truth
						
	11.1°	3.02°	9.70°	3.63°	<b>0.18°</b>	0.00°
						
	4.73°	1.35°	3.86°	7.76°	<b>0.04°</b>	0.00°
						
	5.31°	4.55°	3.71°	3.80°	<b>0.76°</b>	0.00°
						
	7.56°	5.42°	3.77°	4.40°	<b>0.50°</b>	0.00°
						
	5.18°	0.67°	3.69°	3.60°	<b>2.68°</b>	0.00°
						
	4.29°	6.25°	7.03°	5.92°	<b>0.50°</b>	0.00°
						
	4.43°	1.13°	3.73°	4.00°	<b>0.02°</b>	0.00°
(a)	(b)	(c)	(d)	(e)	(f)	(g)

Figure 7. Additional results for illumination chromaticity estimation. (a) Input images. (b/c/d/e/f/g) Illumination corrected images with the chromaticity estimated by using (b) IIC [9], (c) SpePL [2], (d) FacePL [6], (e) FaceGM [1], (f) our method, and (g) calibrated ground truth using a ColorChecker. Below each corrected image is the measured error of the estimated illumination chromaticity.

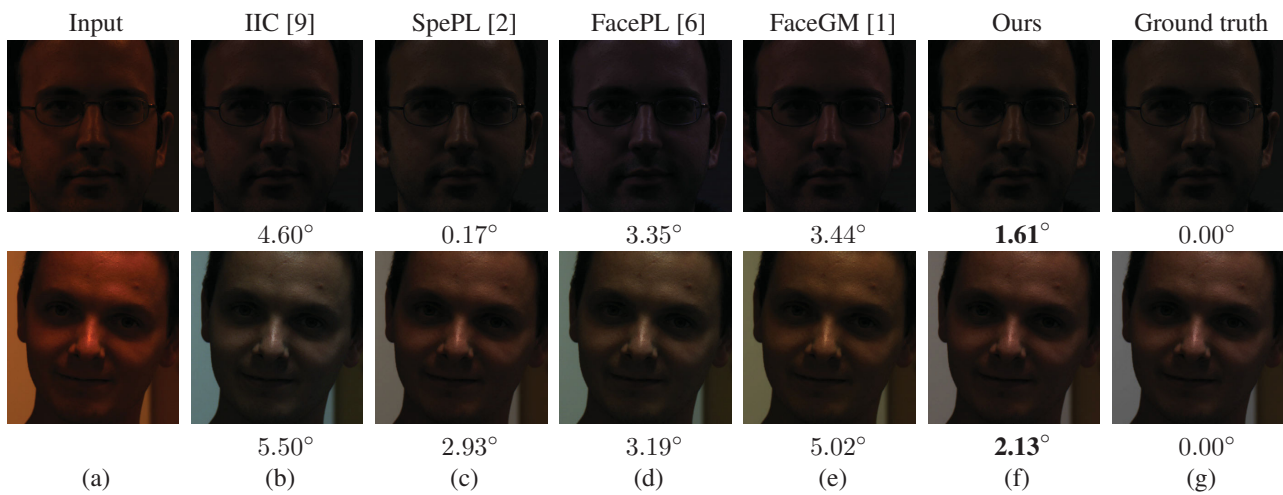
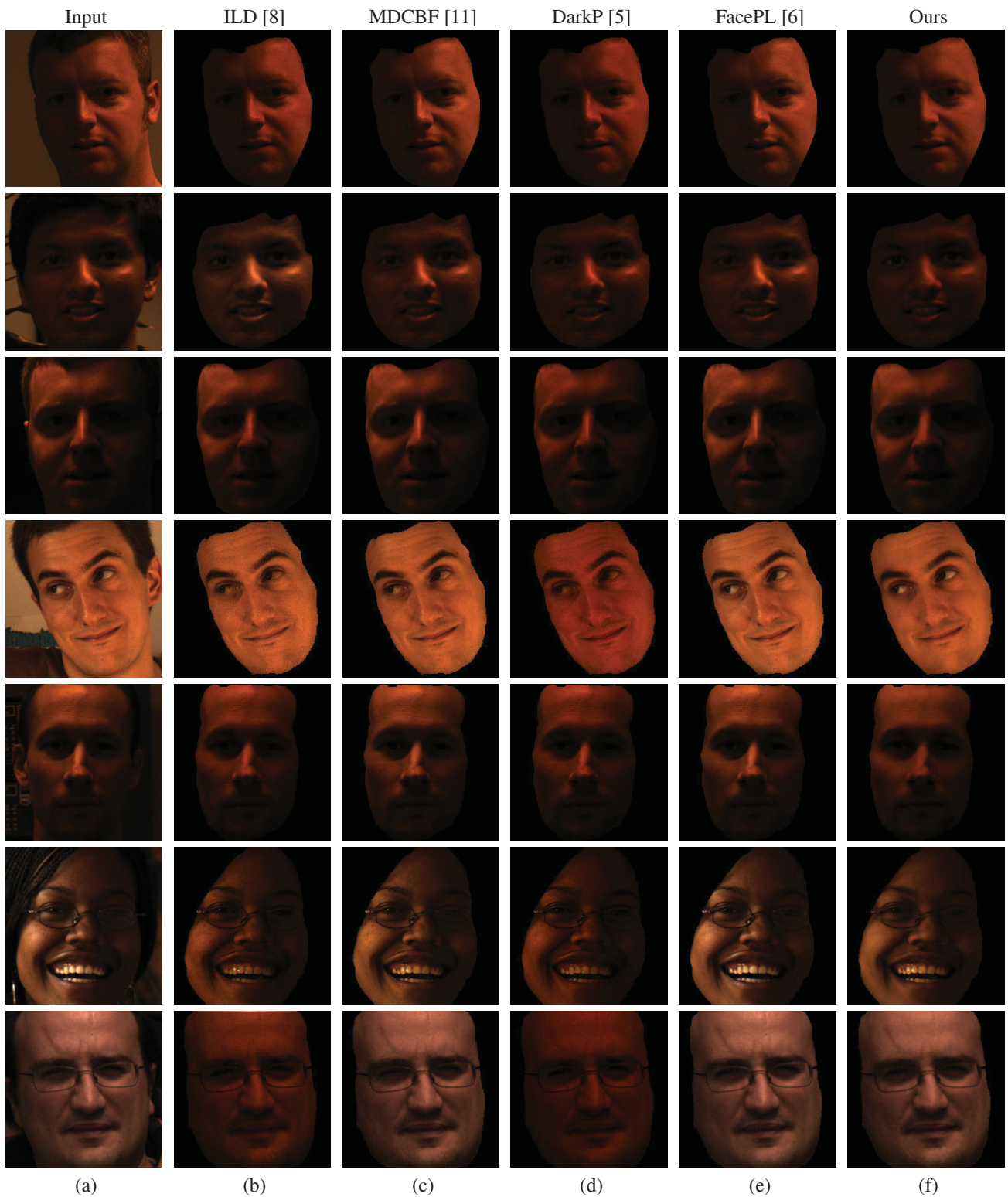


Figure 8. Additional results for illumination chromaticity estimation. (a) Input images. (b/c/d/e/f/g) Illumination corrected images with the chromaticity estimated by using (b) IIC [9], (c) SpePL [2], (d) FacePL [6], (e) FaceGM [1], (f) our method, and (g) calibrated ground truth using a ColorChecker. Below each corrected image is the measured error of the estimated illumination chromaticity.



(a) (b) (c) (d) (e) (f)  
 Figure 9. Additional results for specular highlight removal. (a) Input images. (b/c/d/e/f) Separated diffuse images by (b) ILD [8], (c) MDCBF [11], (d) DarkP [5], (e) FacePL [6], and (f) our method.

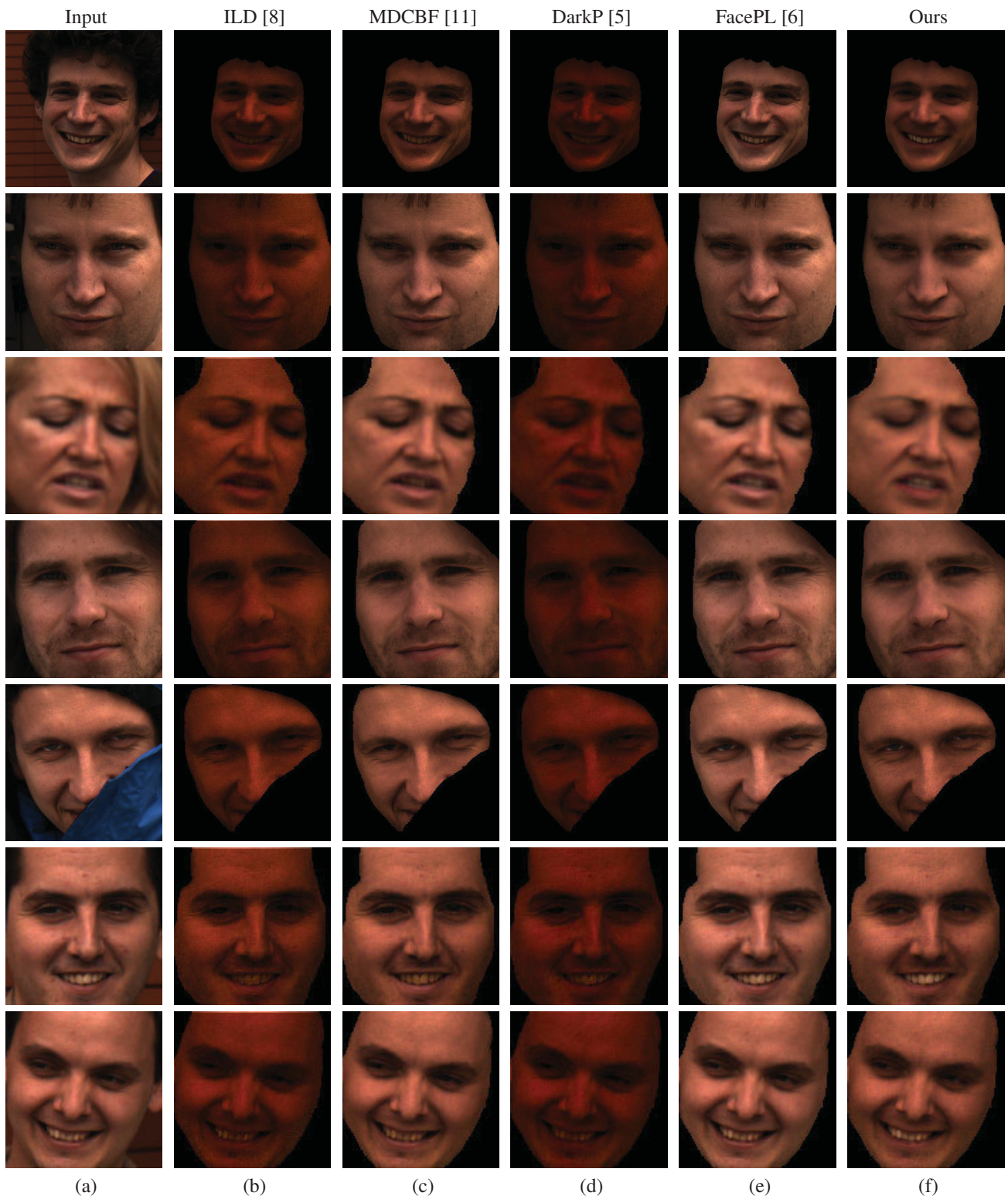


Figure 10. Additional results for specular highlight removal. (a) Input images. (b/c/d/e/f) Separated diffuse images by (b) ILD [8], (c) MDCBF [11], (d) DarkP [5], (e) FacePL [6], and (f) our method.

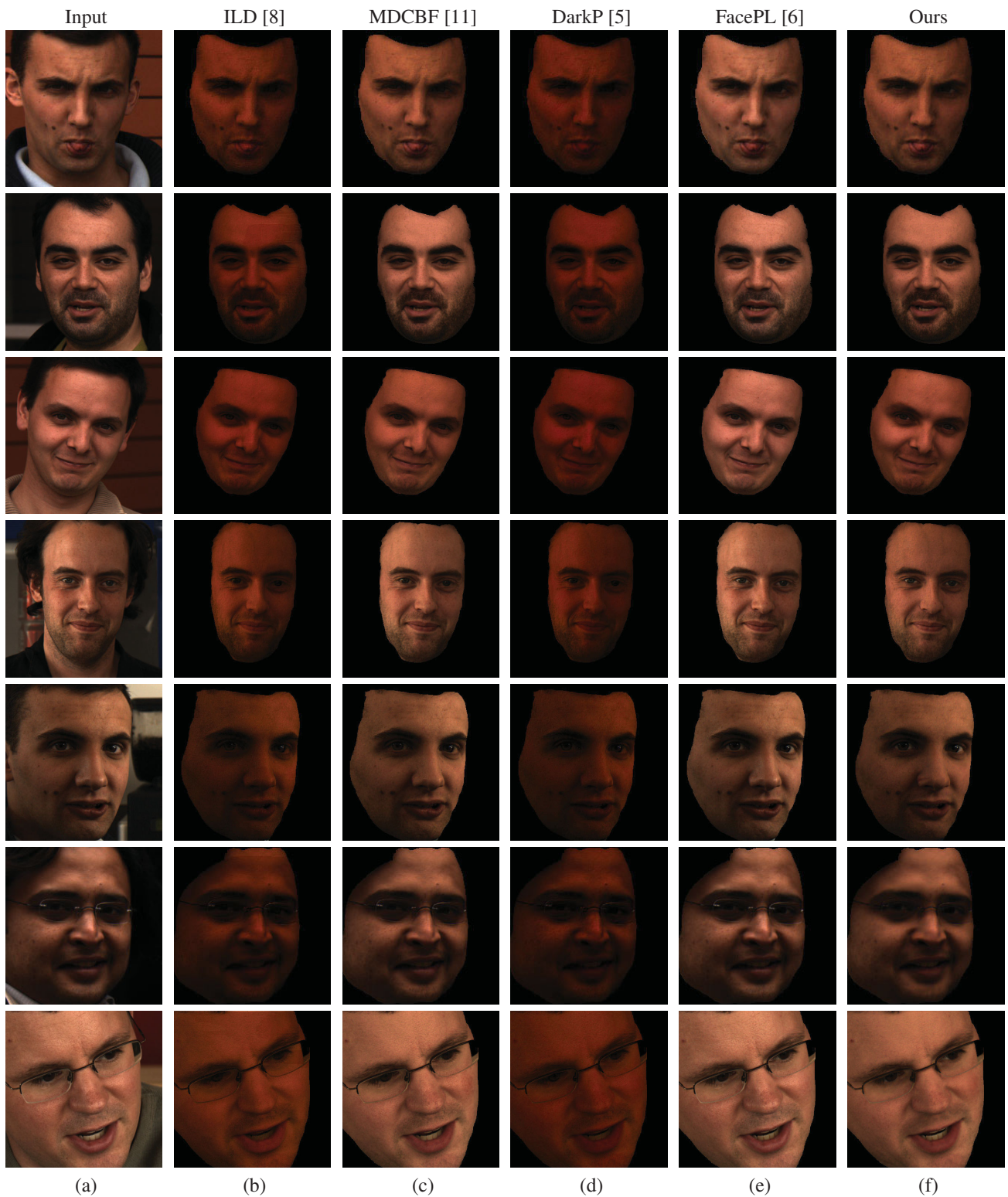
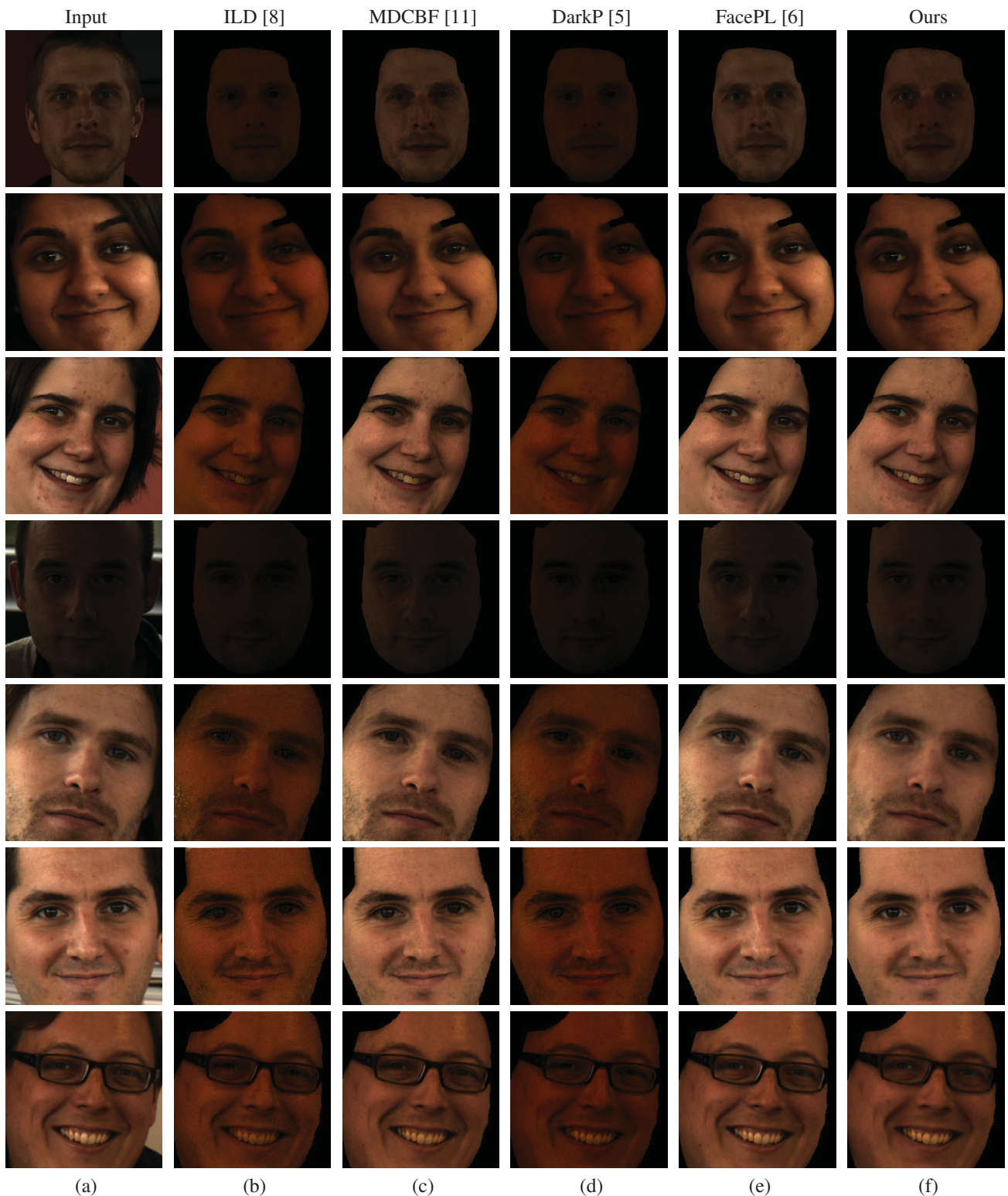
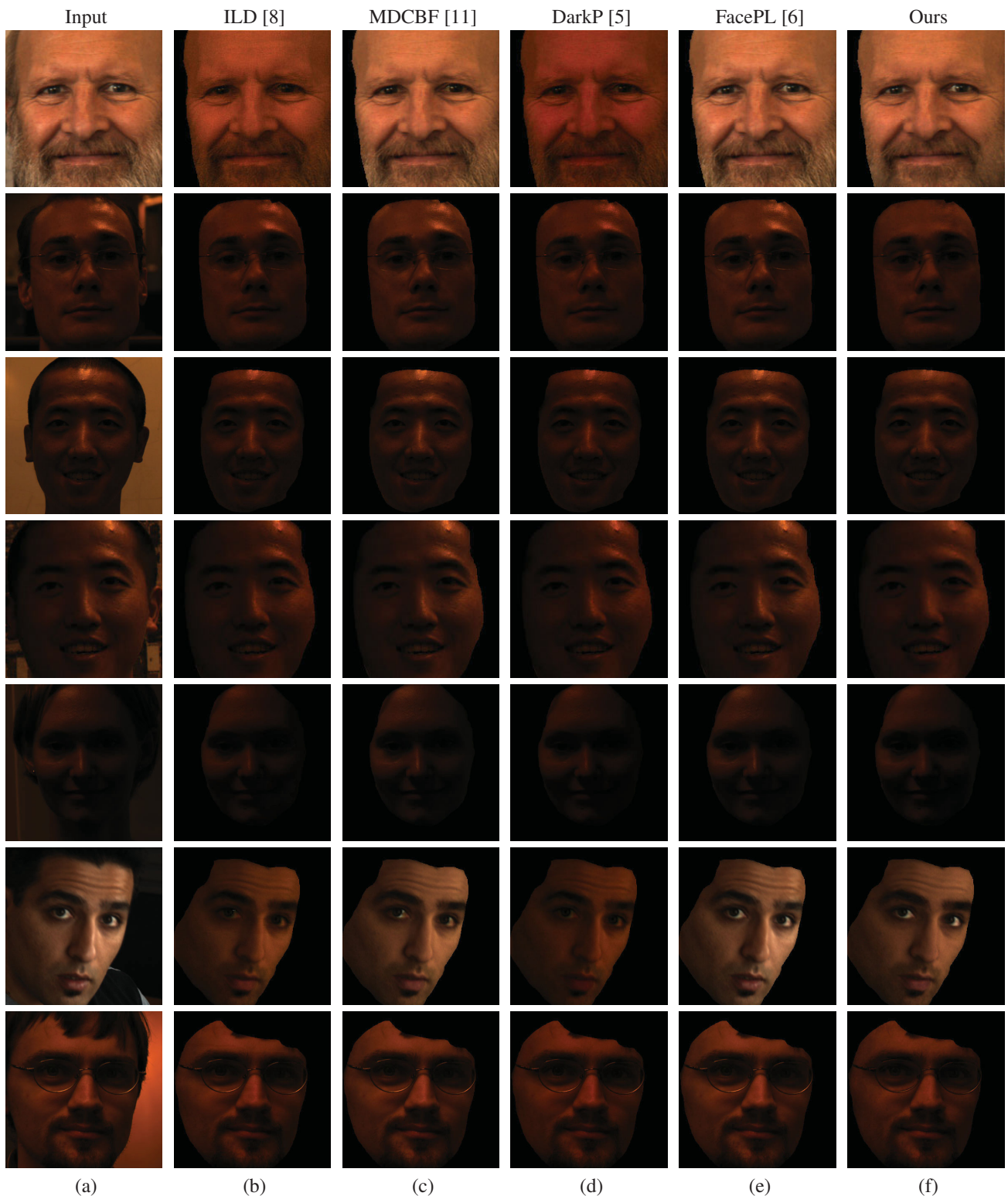


Figure 11. Additional results for specular highlight removal. (a) Input images. (b/c/d/e/f) Separated diffuse images by (b) ILD [8], (c) MDCBF [11], (d) DarkP [5], (e) FacePL [6], and (f) our method.



(a) (b) (c) (d) (e) (f)  
 Figure 12. Additional results for specular highlight removal. (a) Input images. (b/c/d/e/f) Separated diffuse images by (b) ILD [8], (c) MDCBF [11], (d) DarkP [5], (e) FacePL [6], and (f) our method.



(a) (b) (c) (d) (e) (f)  
 Figure 13. Additional results for specular highlight removal. (a) Input images. (b/c/d/e/f) Separated diffuse images by (b) ILD [8], (c) MDCBF [11], (d) DarkP [5], (e) FacePL [6], and (f) our method.

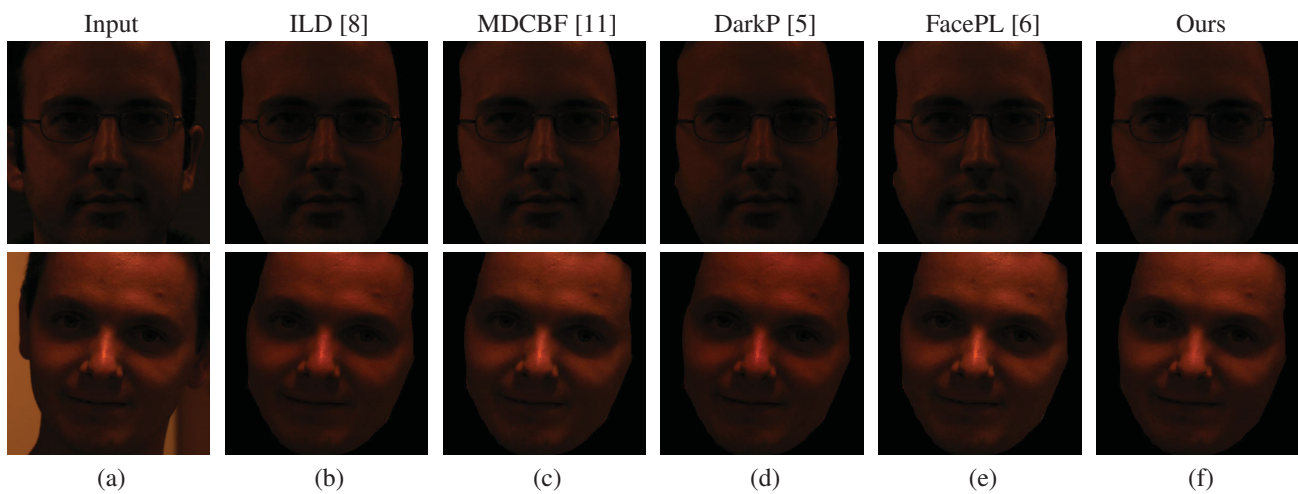


Figure 14. Additional results for specular highlight removal. (a) Input images. (b/c/d/e/f) Separated diffuse images by (b) ILD [8], (c) MDCBF [11], (d) DarkP [5], (e) FacePL [6], and (f) our method.